International Journal of Computer Information Systems and Industrial Management Applications
ISSN 2150-7988 Volume 18 (2026) pp. 1-13

https://doi.org/10.70917/ijcisim-2026-0368
Article

Sustainable Application and Economic Efficiency Analysis of Ship Transportation in the Transportation of Residential Building Materials

Hongwei Li [1,*] and Qiaozi Gao [2]

[1] Maritime College of Guangdong Communications Polytechnic, Guangzhou, Guangdong, 510650, China
[2] School of Maritime Law and Traffic Management, Guangzhou Maritime University, Guangzhou, Guangdong, 510725, China
* Correspondence author: Lhw6469@163.com

Abstract: As a critical link in the supply chain for residential building materials, the sustainability and economic efficiency of shipping play a key role in the low-carbon transformation of the construction industry. This paper establishes a sustainability optimization framework for shipping based on big data analysis and intelligent algorithms, covering key technologies such as ship design and the development of intelligent vessels. A hybrid optimization algorithm combining genetic algorithms and nonlinear programming is proposed to optimize the ship hull form with wave resistance R_w as the objective function. By leveraging augmented reality for real-time, all-around navigation assistance, the study achieves intelligent shipping operations. Using net present value and internal rate of return models, the economic benefits of different transportation scenarios are quantified. Case analyses demonstrate that the optimized ship design reduces resistance by 4.96%, the intelligent navigation system improves visual communication efficiency by 14.29%, and the comprehensive solution achieves over 25% higher economic benefits compared to the baseline.

Keywords: ship transportation; hybrid optimization algorithm; ship hull form optimization; residential building materials; economic benefits

1. Introduction

Residential construction material transportation refers to the process of transporting construction materials from suppliers to construction sites [1]. In construction projects, residential construction material transportation is an indispensable component, directly impacting project progress and quality [2-3]. Therefore, a reasonable residential construction material transportation plan is crucial for the smooth progression of the project [4].

Residential construction materials can be transported via various methods, with the most common being road transport, rail transport, and water transport [5-6]. Road transport is the most widely used method, offering flexibility and convenience, enabling materials to be delivered to any location on the construction site [7-8]. However, road transport also faces challenges such as traffic congestion and poor road conditions [9]. Rail transport is typically suitable for long-distance transportation and the transport of large volumes of materials [10]. Compared to road transport, rail transport has greater capacity, faster speeds, and causes less damage to materials [11]. However, the limitation of rail transport lies in the constraints of railway lines; transportation can only be carried out if railway lines connect to the construction site [12-13]. Water transport is suitable for long-distance transportation and

the transport of materials for large-scale engineering projects [14]. Transportation via waterways such as rivers, canals, or oceans not only allows for the transportation of larger volumes of materials but also effectively reduces transportation costs. Additionally, China has an extremely long coastline, with many excellent ports in coastal regions, providing favorable conditions for maritime transportation activities [15-18]. Furthermore, most residential construction materials are imported, and China's foreign trade continues to expand. As a result, the volume of cargo transported by ships has been increasing, and its significance in the current economy has become increasingly prominent. Therefore, in the transportation of residential construction materials, shipping not only demonstrates sustainability but also offers greater economic benefits compared to other transportation methods [19-22].

This paper first explores big data analysis methods for ship design and proposes optimization strategies to promote sustainable development in the shipping industry. It combines genetic algorithms with nonlinear programming to form a hybrid optimization algorithm for optimizing ship hull shapes. A smart ship navigation assistance system based on augmented reality is designed to achieve efficient ship control and decision-making. A method for evaluating the economic benefits of ship transportation based on net present value is proposed, using the financial indicator internal rate of return to measure the profitability of different transportation modes. A specific inland container ship is selected for analysis to explore the optimization effects of ship transportation. The economic benefits of different schemes are comprehensively compared, and their risk resistance capabilities are assessed using sensitivity analysis.

2. Sustainable design and economic efficiency optimization for ship transportation

2.1. Sustainable Optimization Strategies for Ship Transportation Based on Big Data Analysis

2.1.1. Optimizing ship design

Ship design optimization requires the full utilization of big data throughout the entire lifecycle, from design and construction to operation, collecting massive amounts of data on hull structure, propulsion systems, and operational conditions. By employing big data correlation analysis, the intrinsic relationships between ship hull lines, primary dimensional parameters, and fuel consumption, cargo capacity utilization, and maneuverability are characterized, enabling the construction of multi-scenario energy efficiency models. Building on this foundation, numerical simulation methods such as aerodynamics and computational fluid dynamics are integrated to establish refined simulation models for ship resistance, propulsion, stability, and structural strength. Using intelligent optimization techniques such as multi-objective genetic algorithms, we set fuel consumption, cargo efficiency, stability, and safety as optimization objectives. We conducted parallel optimization of ship hull lines and load distribution, ship hull-propeller-rudder system matching design, and streamlined shaping of the bow and stern appendages, achieving integrated design of the overall ship layout and local details. During the optimization process, intelligent fusion technology combining hydrodynamic model test results and CFD numerical calculations is introduced to achieve closed-loop optimization iteration between simulation and testing, enhancing design efficiency and the reliability of outcomes. This ultimately results in a green ship design that balances indicators such as lifecycle cost, energy efficiency, environmental protection, and safety.

2.1.2. Accelerating the development of smart ships

The development of smart ships first requires the establishment of an IoT system that comprehensively senses the operational status of ships. By installing smart sensors in key areas such as the ship's structure, propulsion system, and cargo equipment, various operational parameters can be collected and transmitted in real time via the ship's communication network to a cloud platform. Second, based on the aggregated big data, machine learning algorithms are used to develop online assessment models for vessel energy efficiency and equipment health status. By analyzing historical energy consumption data and equipment vibration and noise, the system adaptively learns vessel energy efficiency characteristics and equipment fault indicators, enabling real-time monitoring and early warning for energy efficiency and safety. Third, specialized research is conducted on intelligent collision avoidance and energy-saving optimization. By integrating multi-sensor fusion technology to construct a comprehensive perception model and applying deep reinforcement learning to solve optimal collision avoidance strategies, a ship energy consumption mapping model is established. Heuristic

algorithms are used to optimize parameters such as speed, draft, and route, achieving full-process energy-saving control. Finally, the intelligent collision avoidance and energy-saving optimization algorithms are integrated into an intelligent auxiliary decision-making system, forming a ship-shore collaborative autonomous intelligent navigation control solution.

2.2. Optimization design of ship transportation based on intelligent algorithms

2.2.1. Ship hull line optimization design based on hybrid optimization algorithms

In the optimization process, the wave resistance R_w is used as the objective function, and R_w is calculated using the Rankine source method. The free surface mesh is obtained using the streamline tracking method, and the objective function is solved using a mixed optimization algorithm under basic constraint conditions. The mixed optimization algorithm process is shown in Figure 1.

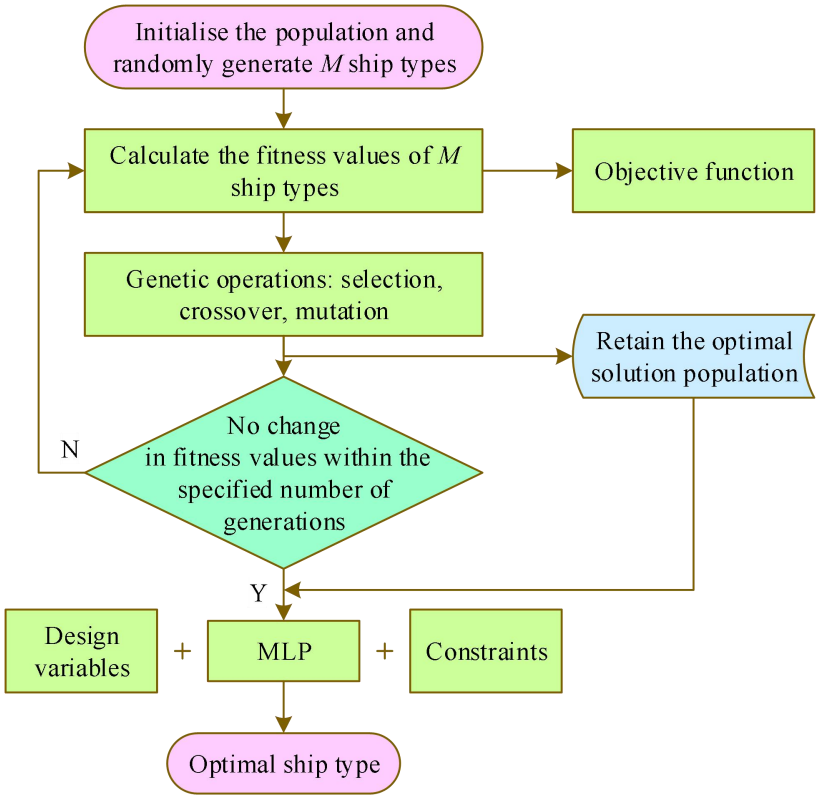

Figure 1. Flow of thc hybrid optimization algorit hm

$$R_w = \frac{1}{2}\rho v^2 L^2 C_w \tag{1}$$

In the formula: C_w is the wave-making resistance coefficient; L is the ship length (length between perpendiculars); ρ is the fluid density; v is the sailing speed.

The optimization model for minimum wave-making resistance can be expressed as:

$$\min R_w \tag{2}$$

$$\left.\begin{aligned} s.t.\ \frac{|\Delta - \Delta_0|}{\Delta_0} \le \varepsilon \\ y(x,z) \ge 0 \end{aligned}\right\} \tag{3}$$

In the equation: Δ_0 and Δ represent the displacement of the parent ship and the modified ship type, respectively; ε is the range of change in the displacement of the modified ship type relative to

the displacement of the parent ship, which is taken as $\varepsilon = 0.6\%$ in this paper; $y(x, z)$ is the ship type value coordinate.

The entire ship is taken as the optimization design range, with the design waterline, ship bottom, and front and rear ends of the design range fixed. The shape of the modified ship type $y(x, z)$ is expressed by multiplying the parent ship type $f_0(x, z)$ by a ship type modification function $w(x, z)$, i.e.:

$$y(x,z) = f_0(x,z) \cdot w_{f,a}(x,z) \tag{4}$$

$$\left.\begin{aligned} w(x,z)_f &= 1 - \sum_m \sum_n a_{mn} \sin\left[\pi\left(\frac{x-x_0}{x_{\min}-x_0}\right)^{m+2}\right] \cdot \sin\left[\pi\left(\frac{z_0-z}{z_0+T}\right)^{n+2}\right] \\ &-L/2 \le x \le 0, \quad m,n = 1,2,\cdots \\ w(x,z)_a &= 1 - \sum_m \sum_n a_{mn} \sin\left[\pi\left(\frac{x-x_0}{x_{\max}-x_0}\right)^{m+2}\right] \cdot \sin\left[\pi\left(\frac{z_0-z}{z_0+T}\right)^{n+2}\right] \\ &0 \le x \le L/2, \quad m,n = 1,2,3 \\ w(x,z) &> 0,\ x > x_0,\ z < z_0 \end{aligned}\right\} \tag{5}$$

In the equation: $w(x,z)_f$ and $w(x,z)_a$ are the hull modification functions for the bow and stern, respectively; x_0, $x_{\max}$ and $x_{\min}$ are the characteristic parameters of the ship shape to be modified; T is the draft. Since $m,n = 1,2,3$ are fixed, there are a total of 18 design variables a_{mn}; therefore, selecting the hull modification functions reduces the number of design variables and improves the optimization calculation speed.

During the calculation process, the penalty function method is used to transform the constrained multi-objective optimization problem into an unconstrained single-objective optimization problem, i.e.,

$$\min\left\{R_w + M_1 \cdot \max\left(0, \frac{|\Delta - \Delta_0|}{\Delta_0} - \varepsilon\right) + M_2 \cdot \sum \max(0, y)\right\} \tag{6}$$

In the formula, M_1 and M_2 are both given maximum numbers.

2.2.2. Design of an Intelligent Ship Navigation Assistance System Based on Augmented Reality

(1) Coordinate Tree Establishment and Conversion

Three-dimensional scene construction typically requires the maintenance of multiple coordinate systems that change over time. The position information obtained by the ship's navigation and positioning system and the target information provided by the AIS are latitude and longitude information in the WGS84 world coordinate system; sensors such as marine radar and laser radar use a three-dimensional Cartesian coordinate system with the sensor position as the origin; the gimbal of the electro-optical tracking system uses a spherical coordinate system; and visible light cameras and infrared thermal imagers use an image pixel coordinate system.

The origin of the Northeast Heaven coordinate system is based on a latitude and longitude grid with a side length of 100 km. The origin is determined by taking the center point of the current grid where the vessel is located and performing a great circle calculation. The spatial transformation matrix between any two sensors can be obtained through physical installation parameters or joint calibration, converting the sensors to the combined navigation carrier coordinate system. The carrier coordinate system is constructed based on the position of the GPS antenna on the vessel, with the origin at the GPS antenna position, forming the vessel's fixed coordinate system O. The bow direction is the Y axis, the starboard direction is the X axis, and the vertical deck upward is the Z axis. The calibration of the camera pixel coordinate system and the electro-optical gimbal coordinate system uses the pinhole model as the camera model. The internal parameters of the electro-optical camera are obtained using Zhang's calibration method. The translation matrix of the external parameters of the electro-optical gimbal is calculated based on the position of the electro-optical gimbal relative to the

Beidou antenna. The basic rotation matrix of the external parameters of the electro-optical gimbal is obtained using the roll angle, pitch angle, and heading angle of the vessel from the integrated navigation observations.

Before overlaying augmented reality virtual symbols on the image data, the original RGB image is first corrected for distortion using the radial distortion correction parameters k_i and tangential distortion correction parameters p_i obtained from the calibration. The camera's internal parameters f_x, f_y, c_x, c_y obtained from calibration, the height h and width w of the image, and the near clipping plane Z_n and far clipping plane Z_f of the projection frustum in the 3D rendering engine, construct the rendering projection matrix K_i that conforms to the camera's internal parameters and the 3D graphics engine:

$$K_i = \begin{bmatrix} \frac{2f_x}{w} & 0 & \frac{w-2c_x}{w} & 0 \\ 0 & -\frac{2f_y}{h} & \frac{h-2c_y}{h} & 0 \\ 0 & 0 & \frac{-(Z_f-Z_n)}{Z_fZ_n(Z_f-Z_n)} & -\frac{2Z_fZ_n}{Z_f-Z_n} \\ 0 & 0 & -1 & 0 \end{bmatrix} \tag{7}$$

By rendering the projection matrix and combining it with the rotation matrix R and translation matrix T published through the coordinate tree, the real-time camera extrinsic parameters K_e are obtained:

$$K_e = \begin{bmatrix} R_{3\times3} & T_{3\times1} \\ 0_{3\times3} & 1 \end{bmatrix} \tag{8}$$

The conversion relationship between the northeast sky coordinates (x, y, z) and the camera pixel coordinates (p_x, p_y) can be obtained:

$$\begin{bmatrix} p_x & p_y & 1 \end{bmatrix}^T = \frac{1}{z_c} K_i K_e \begin{bmatrix} x & y & z & 1 \end{bmatrix}^T \tag{9}$$

In the equation: z_c is the position variable.

By establishing a transform (TF) publisher node in ROS to publish the coordinate system transformation matrix, spatial synchronization of heterogeneous multi-sensor data is achieved.

(2) Collision avoidance warning

In the process of handling dynamic and static targets during navigation collision avoidance, a decision-level fusion method is used for single-sensor detection results. The dynamic fusion process is as follows: whenever the sensor perceives the latest observation information of the updated target, the Euclidean distance between each perception information and the fused target is calculated based on the obstacle information and the static object information on the electronic chart through the relative distance, bearing, heading, and speed of the ship. A fuzzy multi-factor set and evaluation matrix are then established.

$$R = \begin{bmatrix} r_d(k) & r_\theta(k) & r_{cog}(k) & r_{sog}(k) \end{bmatrix}^T \tag{10}$$

In the formula, $r(k)$ is the association membership function of the fuzzy factor set, calculated as follows:

$$r(k) = exp\left(-\tau_q(u_q^2(k)/\sigma_q^2)\right) \tag{11}$$

Based on the association matrix R, the multi-sensor matching degree is calculated using the minimum distance cost.

Since the image lacks distance dimension information, only the pixel range of the ship in the image can be obtained. By detecting the horizon line, the ship image is segmented, and the pixel range of the image recognition target obtained through the YOLO algorithm is matched and associated with the

pixel bounding box of the fusion target after coordinate transformation based on the intersection over union (IOU) to obtain the correlation matching information between the optical image and the fusion target.

Accurate ship collision hazard warnings are a prerequisite for ensuring safe navigation and effective avoidance. Collision risk warning is performed by calculating the collision risk index (CRI). The collision risk index is a measure of the likelihood of a collision between two vessels, determined using the initial distance of approach (DCPA), the bearing of the initial closest point of approach (CPA), the safe passing distance, and the minimum safe distance of approach, based on a fuzzy mathematics evaluation method. When the target CRI reaches the set thresholds CRI_0 and CRI_1, a three-level collision avoidance warning is issued through sound and label color: alert, caution, and danger.

2.3. Methods for assessing the economic benefits of shipping

Net Present Value (NPV) refers to the difference between the present value of future cash inflows and the present value of future cash outflows. It is the fundamental indicator in the NPV method used for project evaluation. Both future cash inflows and outflows are converted to present value using the discount rate and present value factors for each period, after which the net present value is determined. If the net present value is positive over the project's lifecycle, it indicates that the project has investment value; otherwise, it does not. The earlier the NPV becomes positive, the higher the project's investability.

The calculation method for NPV is shown in Equation (12).

The following is the entered content:

$$NPV = \sum_{t=0}^{T} \frac{CF_t}{(1+r)^t} - C_0 \tag{12}$$

In this context, T represents the transportation lifecycle in years, CF_t denotes the net cash flow in operational year t, and C_0 signifies the capital investment. r refers to the discount rate, which is the interest rate used to discount future cash flows to the present point. It is typically determined by factors such as the risk of the investment project and market interest rates.

This paper conducts an economic analysis as close to reality as possible, taking into account the tax rate TR. Equation (12) can be replaced by Equation (13).

$$NPV = (1-TR)\sum_{t=0}^{T} \frac{REV_t - OPEX_t}{(1+r)^t} - C_0 \tag{13}$$

Among them, REV_t represents the product sales revenue in operating year t, and $OPEX_t$ represents the operating and maintenance expenses incurred in operating year t. TR is the tax rate levied on net income.

Product sales revenue can be expressed by equation (14).

$$REV = M_{H_2} \cdot (1-ERD)^t \cdot U_{NH_3} \tag{14}$$

Among them, M_{H2} represents the annual production and transportation of hydrogen, and ERD represents the equipment depreciation rate.

The normalized hydrogen production cost is calculated by first normalizing the costs and hydrogen production volume over the project's life cycle, and then calculating the hydrogen production cost, i.e., the present value of the costs over the life cycle divided by the present value of the hydrogen production volume over the life cycle. The calculation method is shown in Equation (15).

$$\begin{aligned} LCOH &= \frac{Total\ lifetime\ \text{cost}}{Total\ lifetime\ H_2\ production} \\ &= \frac{C_0 + TR\sum_{t=0}^{T} \frac{REV_t - OPEX_t}{(1+r)^t} + \sum_{t=0}^{T} \frac{OPEX_t}{(1+r)^t} - C_j}{\sum_{t=0}^{T} \frac{M_{H_2} \cdot (1-ERD)^t}{(1+r)^t}} \end{aligned} \tag{15}$$

Among these, C_j represents the present value of the residual value of fixed assets. In this study, it refers to the construction costs of offshore wind farms and synthetic ammonia plants. This study

primarily focuses on transportation scenario analysis; however, the calculation of hydrogen equilibrium prices cannot exclude hydrogen production costs. Therefore, this study treats offshore wind farm investments as fixed assets.

The levelized hydrogen production cost is not a simple arithmetic operation but is influenced by numerous factors. Under different transportation scenarios, the final levelized hydrogen production cost varies. Based on this indicator, the study can systematically compare the advantages of different transportation modes and optimize them accordingly.

In addition to net present value (NPV) calculations, this study also employs the financial metric internal rate of return (IRR) to assess the profitability of different transportation modes. NPV calculations may not fully account for differences in investment scale between modes, while the IRR is the rate of return that equates the present value of capital inflows to the total value of capital inflows and sets the NPV to zero. A higher IRR indicates stronger project profitability. If a project's IRR

is equal to or greater than the benchmark rate of return (BRR), the project is generally considered feasible. In short, profits can only be generated when the internal rate of return exceeds the discount rate (r). By analyzing the internal rate of return, scenario comparisons and decision-making can be conducted more effectively. The higher the internal rate of return, the stronger the competitiveness of the transportation mode in this scenario.

This study uses Equation (16) to calculate the internal rate of return.

$$\sum_{t=0}^{T} \frac{CF_t}{(1+IRR)^t} = 0 \tag{16}$$

During the operational lifespan of a project, it is necessary to consider the risk associated with its operational year returns. The risk-free rate (r_f) refers to the rate of return on investments that carry no risk in the market. Based on the assumptions of this study, it is assumed to be 2%. When the risk rate exceeds 2%, it constitutes a risk premium. This means that the risk rate of the operational project exceeds the expected return value of the risk-free rate r_f . Under r_f , the expression for the present value of cash flows PV_E can be represented by Equation (17).

$$PV_E = \frac{\alpha_E \cdot X}{1+r_f} \tag{17}$$

Among them, α_E represents the deterministic equivalence coefficient, with a value greater than 1. X is the expected income value.

Similarly, the actual cash flow PV_o for the operating year can be expressed by equation (18).

$$PV_o = \frac{\alpha_o \cdot X_o}{1+r_o} \tag{18}$$

In this study, the cash flow for the operating year is CF_t , and the expected value can be set as the revenue REV for the operating year t when the equipment depreciation rate ERD is 0. Therefore, the risk rate r_o for the actual operating year can be derived, as shown in Equation (19).

$$r_o = \frac{\alpha_o \cdot X_o}{CF_t} - 1 = \frac{REV}{CF_t} - 1 \tag{19}$$

3. Analysis of the effectiveness of the optimized design plan for ship transportation

3.1. Analysis of the effects of hull shape optimization

Taking a certain inland river container ship as an example, the hull form optimization was conducted at a design speed of F=0.205. The calculations were based on the ship model scale and the main hull parameters of the actual ship, as shown in Table 1. The actual ship has a waterline length of 125.47 meters, a beam of 19.35 meters, a draft of 4.62 meters, a square coefficient of 0.8536, and a diamond coefficient of 24.26. After scaling down the ship model proportionally, the waterline length is 6.028 meters, the beam is 0.846 meters, and the draft is 0.201 meters. These parameters provide the foundational design basis for subsequent hull form optimization.

Table 1. Main ship type Parameters

	Waterline length/m	Type width/m	Drink water	Square coefficient	Shrinkage ratio
Actual vessel	125.47	19.35	4.62	0.8536	24.26
Model ship	6.028	0.846	0.201		

The optimization process employs the hybrid optimization algorithm mentioned in the article, and the results of the hull optimization are shown in Table 2. After optimization, the wave-making resistance of the hull decreased by 5.13%, and the total resistance decreased by 4.96%, achieving the goal of automatic hull shape optimization.

Table 2. Results of Hull Optimization

Ship type	Wave resistance coefficient	Total resistance coefficient	Floating heart position	Drainage volume	Wet surface area
	Cw	Ct	Lcb	D(t)	S
Mother type	7.036E-04	3.975E-03	0.503	0.704	6.363
Optimization	6.675E-04	3.778E-03	0.481	0.716	6.512
Comparison	Reduce 5.13%	Reduce 4.96%	Change 4.37%	Change 1.70%	Change 2.34%

To validate the hydrodynamic characteristics of the optimized hull design, numerical simulation and modeling of the hull's wake resistance were conducted using the Fluent software platform and Gambit mesh generation tool. The simulation results for wake resistance at different locations on the vessel are shown in Figure 2. At Position A, a distinct positive resistance peak is observed in the bow region, while the midship to stern regions exhibit a negative resistance distribution. At Position B, the maximum positive resistance value reaches 0.0035, and the minimum negative resistance value reaches -0.0038. The regions of extreme resistance values at both positions are located where the hull curvature changes significantly, confirming the regulatory effect of the optimized hull design on the wave-making resistance distribution.

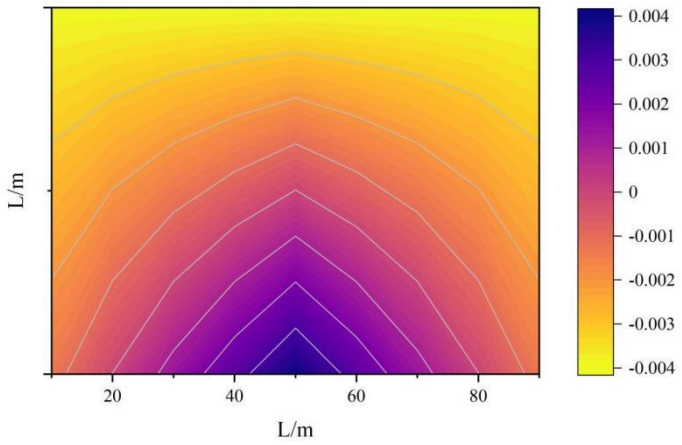

(a)Position A

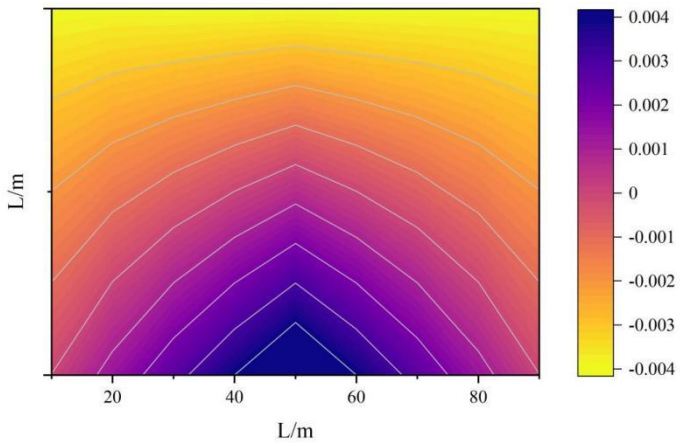

(b)Position B

Figure 2. Simulation results of wave resistance at different positions

3.2. Analysis of Navigation System Effectiveness

Under the condition of overall functional realization, simulation experiments were conducted during the ship's voyage. The yaw angle and voyage speed errors during the simulation are shown in Figure 3. It can be seen that during the simulation, as the voyage distance increased, both the yaw angle and voyage speed errors remained within controllable ranges. The yaw angle error stabilized between 2.5° and 5°, while the voyage speed error remained within 0.5 m/s.

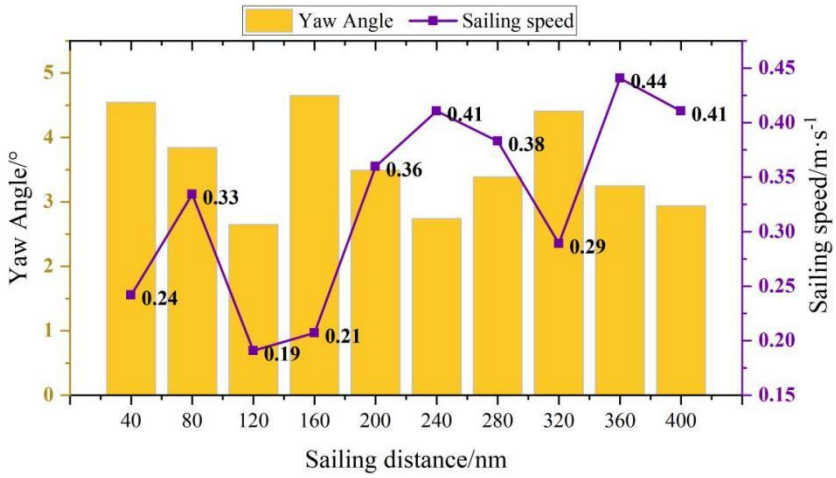

Figure 3. Navigation error results

To analyze the optimization effects of visual communication before and after the use of an augmented reality-based intelligent ship navigation assistance system, we tested the mean pupil diameter, mean gaze duration, and visual communication index of different staff members before and after adopting the navigation system described in this paper. The results of the visual communication effectiveness test are shown in Table 3. It can be seen that the AR-based intelligent ship navigation assistance system designed using the method described in this paper resulted in smaller mean pupil diameters and mean fixation times for staff members, with an average visual communication index 14.29% higher than before use, demonstrating that the method effectively optimizes the visual communication effectiveness of ship intelligent navigation human-machine interaction.

Table 3. Test Results of Visual Communication Effect

Staff member	Before			After		
	Mean pupil diameter/px	Mean fixation time/s	Visual Communication Index	Mean pupil diameter/px	Mean fixation time/s	Visual Communication Index
X1	63.64	35.49	0.99	78.47	46.36	0.84

X2	62.17	34.92	0.97	77.42	45.18	0.86
X3	63.44	33.88	0.98	76.94	46.77	0.85
X4	61.08	34.51	0.99	78.15	47.32	0.83
X5	63.22	35.03	0.98	77.63	46.38	0.88
X6	61.94	33.68	0.97	78.06	47.59	0.81
X7	60.98	32.75	0.99	79.13	47.11	0.84
X8	61.37	33.26	0.97	78.54	48.35	0.83
Mean value	62.23	34.19	0.98	78.04	46.8825	0.84

3.3. Economic Benefit Assessment

3.3.1. Comprehensive Comparison

This section will conduct economic benefit calculations for different remediation schemes based on the proposed model. The calculations reference fuel prices, speed, and other data provided by relevant research institutions, and statistical calculations are performed based on historical data. Assuming the construction year is 2024, Scheme 1 involves optimizing the ship's hull form using a hybrid optimization algorithm, while Scheme 2 is the optimization scheme proposed in this paper. The economic benefits before and after optimization for both schemes are compared as shown in Tables 4 and 5. After implementing Scheme 1, the improvement in downward economic benefits ranges from 25% to 55%, and the improvement in upward economic benefits ranges from 20% to 50% between 2025 and 2045, with the most significant improvement in downward economic benefits occurring in 2040. As a comprehensive optimization scheme, Scheme 2 demonstrates more significant improvements in economic benefits. The average increase in downward economic benefits across all years is 1.74 percentage points higher than Scheme 1, and the average increase in upward economic benefits is 1.53 percentage points higher, validating the advantages of the synergistic effects between hull form optimization and the intelligent navigation system.

Table 4. Comparison of Economic Benefits of Scheme One

Economic benefit	**Before /100 million yuan**		**After /100 million yuan**		**Save the proportion of economic benefits/%**	
	Downward	**Upward**	**Downward**	**Upward**	**Downward**	**Upward**
2025	2.57	2.62	3.25	3.91	26.46	49.24
2030	3.01	3.62	3.74	4.36	24.25	20.44
2035	2.93	3.71	3.78	4.82	29.01	29.92
2040	2.65	3.73	3.99	4.98	50.57	33.51
2045	2.77	3.75	4.04	5.06	45.85	34.93

Table 5. Comparison of Economic Benefits of Plan Two

Economic benefit	**Before /100 million yuan**		**After /100 million yuan**		**Save the proportion of economic benefits/%**	
	Downward	**Upward**	**Downward**	**Upward**	**Downward**	**Upward**
2025	2.57	2.62	3.31	3.94	28.79	50.38
2030	3.01	3.62	3.78	4.45	25.58	22.93
2035	2.93	3.71	3.83	4.91	30.72	32.35
2040	2.65	3.73	4.05	5.02	52.83	34.58
2045	2.77	3.75	4.07	5.08	46.93	35.47

3.3.2. Sensitivity Analysis

When conducting a sensitivity analysis of a project, it is important to consider how economic evaluation indicators may change under adverse conditions to determine whether the project possesses a certain level of risk resistance. In this analysis, three scenarios will be considered: cost increases, revenue decreases, and simultaneous cost increases and revenue decreases. Net present value (NPV), benefit-cost ratio (BCR), internal rate of return (IRR), and payback period will be calculated for each scenario. The results of the sensitivity analysis for the two schemes are shown in Tables 6 and 7, respectively. Under the base case scenario, the net present values for Scenario 1 and Scenario 2 are 2.016 billion yuan and 4.939 billion yuan, respectively, with benefit-cost ratios of 2.23 and 3.17, and internal rates of return of 16.36% and 16.45%, respectively, all exceeding the 10% benchmark discount

rate. When costs increase by 12%, the net present value of Option 2 decreases by 4.05%, which is smaller than the 1.49% decrease for Option 1, indicating its stronger cost resilience. In a scenario where revenues decrease by 12%, the benefit-cost ratio of Option 2 remains at 2.13, significantly higher than the 1.62 for Option 1. Under the most unfavorable scenario, the payback period for Scheme 2 increases by 1.51 years, a larger increase than the 0.47 years for Scheme 1, but its absolute value remains within an acceptable range, primarily due to its higher initial investment scale. Overall, the optimized scheme in this paper demonstrates a clear absolute benefit advantage under the benchmark scenario, and its key indicators remain within industry-acceptable levels across various scenarios.

Table 6. Results of sensitivity analysis for Scheme One

Evaluation index	ENPV (I=10%)	EBCR (I=10%)	EIRR/%	Pt/year
The cost has risen by 0%	2016465355.35	2.23	16.36	10.22
The cost has risen by 12%	1986443445.41	2.15	14.73	10.31
The efficiency has decreased by 12%	1794753575.62	1.62	14.66	10.45
The cost rose by 12% and the benefit dropped by 12%	1586333683.48	1.94	13.42	10.69

Table 7. Results of sensitivity analysis for Scheme Two

Evaluation index	ENPV (I=10%)	EBCR (I=10%)	EIRR/%	Pt/year
The cost has risen by 0%	4938646443.75	3.17	16.45	10.98
The cost has risen by 12%	4738465593.27	3.02	15.36	11.27
The efficiency has decreased by 12%	4026464822.43	2.13	15.34	12.05
The cost rose by 12% and the benefit dropped by 12%	4027568643.48	2.64	14.27	12.49

4. Conclusion

This study employs a dual-track analysis combining technological innovation and economic modeling to demonstrate that ship transportation offers both environmental and economic benefits in the transportation of residential building materials.

A hybrid optimization algorithm was used to optimize the ship's hull form, resulting in a 5.13% reduction in wave-making resistance and a 4.96% reduction in total resistance, achieving the goal of automatic hull form optimization. In navigation system simulation experiments, as the voyage distance increased, both the yaw angle error and voyage speed error remained within controllable ranges. The yaw angle error stabilized between 2.5° and 5°, while the voyage speed error remained within 0.5.

Using the optimization design proposed in this paper, the economic benefits in each year showed an average increase of 1.74 percentage points in downward economic benefits and 1.53 percentage points in upward economic benefits compared to Scheme 1. The net present value decreased by 4.05%, which is smaller than the 1.49% decrease in Scheme 1. Under a scenario where revenue decreases by 12%, the benefit-cost ratio of Scheme 2 remains at 2.13, significantly higher than the 1.62 of Scheme 1. Under the most unfavorable scenario, the payback period for Scheme 2 is extended by 1.51 years, a larger increase than the 0.47-year extension for Scheme 1, but its absolute value remains within an acceptable range. Overall, the optimized scheme proposed in this paper demonstrates a clear absolute benefit advantage under the baseline scenario, and its key indicators remain within industry-acceptable levels across various scenarios.

Funding

This research was supported by the:

2023 Guangdong Provincial Education Science Planning (Higher Education Special Project) Project "Research on the Transformation and Upgrading of Talent Training System for Transportation Majors in Higher Vocational Education under the Digital Background" (No. 2023GXJK747); The Fourth Council of Guangdong Vocational and Technical Education Association's 2023-2024 Research Plan Project "Research on the Mechanism of Technological Achievement Transformation in Vocational Colleges from the Perspective of Collaborative Innovation" (No. 202212G063); Education Science Research Project of China Transportation Education Research Association for 2022-2024 (JT2022ZD045); 2022 Education and Teaching Reform and Practice Project of Guangdong Vocational College Integration Work Guidance Committee (No. 2022CJRH09); The 2023 Education and Teaching Reform Research and Practice Project of Guangdong Vocational College Electronic Information and

Communication Teaching Guidance Committee (No. 21); School level Project "Practical Research on Enhancing the Digital Teaching Ability of Vocational College Teachers and Constructing an Evaluation System under the Background of Digital Transformation" (No. GDCP-ZX-2022-011-N1).

References

1. Cha, G. W., Hong, W. H., & Kim, J. H. (2017). A study on CO2 emissions in end-of-life phase of residential buildings in Korea: demolition, transportation and disposal of building materials. Key Engineering Materials, 730, 457-462.
2. Jonnala, S. N., Gogoi, D., Devi, S., Kumar, M., & Kumar, C. (2024). A comprehensive study of building materials and bricks for residential construction. Construction and building materials, 425, 135931.
3. Peng, Z., Deng, W., & Hong, Y. (2019). Materials consumption, indoor thermal comfort and associated energy flows of urban residential buildings: case studies from the cold climate zone of China. International Journal of Building Pathology and Adaptation, 37(5), 579-596.
4. Ben-Alon, L., Loftness, V., Harries, K. A., DiPietro, G., & Hameen, E. C. (2019). Cradle to site Life Cycle Assessment (LCA) of natural vs conventional building materials: A case study on cob earthen material. Building and Environment, 160, 106150.
5. Jiangnan, L. (2024). Road Transportation Development, Application of. In The ECPH Encyclopedia of Mining and Metallurgy (pp. 1800-1800). Springer, Singapore.
6. Bešinović, N. (2020). Resilience in railway transport systems: a literature review and research agenda. Transport Reviews, 40(4), 457-478.
7. Rigogiannis, N., Bogatsis, I., Pechlivanis, C., Kyritsis, A., & Papanikolaou, N. (2023). Moving towards greener road transportation: A review. Clean Technologies, 5(2), 766-790.
8. Chai, J., Lu, Q. Y., Wang, S. Y., & Lai, K. K. (2016). Analysis of road transportation energy consumption demand in China. Transportation Research Part D: Transport and Environment, 48, 112-124.
9. Chen, Z., Antunes, J., Wanke, P., & Zhou, M. (2021). Sustainability drivers in road transportation system: Evidence from China. Science of the total environment, 798, 149259.
10. Jalolova, M., Amirov, L., Askarova, M., & Zakhidov, G. (2022). Territorial features of railway transport control mechanisms. Transportation Research Procedia, 63, 2645-2652.
11. Song, M., Zhang, G., Zeng, W., Liu, J., & Fang, K. (2016). Railway transportation and environmental efficiency in China. Transportation Research Part D: Transport and Environment, 48, 488-498.
12. Ghaviha, N., Campillo, J., Bohlin, M., & Dahlquist, E. (2017). Review of application of energy storage devices in railway transportation. Energy Procedia, 105, 4561-4568.
13. Niu, Y., Li, X., Zhang, J., Deng, X., & Chang, Y. (2023). Efficiency of railway transport: A comparative analysis for 16 countries. Transport Policy, 141, 42-53.
14. Kjärstad, J., Skagestad, R., Eldrup, N. H., & Johnsson, F. (2016). Ship transport—A low cost and low risk CO2 transport option in the Nordic countries. International Journal of Greenhouse Gas Control, 54, 168-184.
15. Peng, P., Cheng, S., Chen, J., Liao, M., Wu, L., Liu, X., & Lu, F. (2018). A fine-grained perspective on the robustness of global cargo ship transportation networks. Journal of Geographical Sciences, 28, 881-889.
16. Ferrari, C., & Tei, A. (2020). Effects of BRI strategy on Mediterranean shipping transport. Journal of Shipping and Trade, 5(1), 14.
17. Melnyk, O., Onyshchenko, S., Onishchenko, O., Shumylo, O., Voloshyn, A., Koskina, Y., & Volianska, Y. (2022). Review of ship information security risks and safety of maritime transportation issues. TransNav: International Journal on Marine Navigation and Safety of Sea Transportation, 16.
18. Wang, C., Mao, Y. S., Hu, B. Q., Deng, Z. J., & Shin, J. G. (2016). Ship Block Transportation Scheduling Problem Based on Greedy Algorithm. Journal of Engineering Science & Technology Review, 9(2).

19. Gu, Y., Dong, X., & Chen, Z. (2020). The relation between the international and China shipping markets. Research in Transportation Business & Management, 34, 100427.
20. Watson, A. (2020). Transport in transition: The evolution of traditional shipping in China (p. 113). University of Michigan Press.
21. Sun, Y., Lu, Z., Lian, F., & Yang, Z. (2023). Study of channel upgrades and ship choices of river-shipping of port access-transportation. Transportation Research Part D: Transport and Environment, 119, 103733.
22. Guo, L., & Yang, Z. (2019). Relationship between shipping accessibility and maritime transport demand: the case of mainland China. Networks and Spatial Economics, 19, 149-175.